Supporting Information

Phosphorus Dopants Triggered Single-atom Platinum Catalysis for Efficient Hydrogen Evolution in Proton Exchange Membrane Electrolyzers

Jin Peng[a#], Zhen Wang[a#], Kang Jiang[a], Ming Peng[a], Nithyadharseni Palaniyandy[b], Jianwei Ren[c], Yongwen Tan[a]*

[a]College of Materials Science and Engineering, Hunan University, Changsha, Hunan 410082, China

[b]Institute for Catalysis and Energy Solutions (ICES), College of Science, Engineering, and Technology (CSET), University of South Africa, Florida Science Campus, Roodepoort, 1709, South Africa

[c]Department of Chemical Engineering, Faculty of Engineering, Built Environment and Information Technology, University of Pretoria，Hatfield 0028，Pretoria, South Africa

[#]These authors contributed equally to this work

*Corresponding author

E-mail: tanyw@hnu.edu.cn (Y. Tan)

Experimental section

Synthesis of Catalysts

Synthesis of NPG:

NPG was obtained through etching away the Ag from $Au_{35}Ag_{65}$ nanosheet by etching it for 8h in 30 mL of 65-68% mass fraction HNO_3.[1, 2]

Synthesis of np-MoS_2:

The MoS_2@NPG composite structure was synthesized by CVD in a three-zone tubular furnace. Subsequently, the MoS_2@NPG composite structure was etched to remove NPG by KI-I_2 solution (24 mg I_2 and 12 mg KI dissolved in 100 mL deionized water) for 24 h to obtain np-MoS_2.

Synthesis of P/np-MoS_2:

Subsequently, P/np-MoS_2 was synthesized by further CVD in a two-zone tubular furnace. 1.0 g of $NaH_2PO_2 \cdot H_2O$ was placed in the upstream position, and the obtained MoS_2@NPG composite structure was placed in the downstream position, and the temperature zone where $NaH_2PO_2 \cdot H_2O$ located was subsequently heated to 300 °C at a rate of 3 °C min^{-1} and held for 2 h under the conditions of 90 sccm of Ar and 10 sccm of H_2, meanwhile the temperature zone where the MoS_2@NPG composite structure located was heated to 500 °C at a rate of 5 °C min^{-1} and held for 2 h. P/MoS_2@NPG composite structure was obtained by natural cooling, followed by etching away the NPG to obtain P/np-MoS_2.

Synthesis of Pt_{SA}, P/np-MoS_2:

Initially, 2 mg of $H_2PtCl_6 \cdot 6H_2O$ was dissolved in 50 mL of deionized water and stirred for 1 h to ensure uniform dispersion of H_2PtCl_6, followed by immersion of the obtained P/np-MoS_2 sheet into it at room temperature for 12 h. The obtained sheet was then transferred to carbon cloth and dried naturally at room temperature and atmospheric pressure for 10 h. Finally, the sheet was placed in a vacuum drying oven at 60 °C for 12 h to obtain the Pt_{SA}, P/np-MoS_2.

Synthesis of Pt_{SA}/np-MoS_2:

A similar method was employed to transfer the np-MoS_2 sheet to the same concentration of H_2PtCl_6 solution and then dried in the same process mentioned above to obtain a comparison sample of Pt_{SA}/np-MoS_2.

Structural characterizations

The microscopic morphology of the prepared catalysts was identified by SEM (JEOL, JSM-7610FPlus) with a volt of 10 kV. HAADF-STEM and EELS of the as-obtained catalysts were characterized by TEM (Thermo Scientific, Themis Z) equipped with a focused ion beam (Thermo Scientific, Helios 5 CX). The chemical structure and phase characteristics of all the samples are analyzed by Raman spectroscopy (Witec Alpha300R) with an excitation wavelength of 488 nm. The chemical state and electronic structure of the catalysts were carried out by XPS (Thermo Scientific ESCALAB250Xi spectrometer with the monochromatic Al Kα). ICP-OES was performed on an Agilent 730 to obtain the content of elements in the sample. The Pt L_3-edge and Mo K-edge XAS spectra were probed at the beamline BL01C1 of National Synchrotron Radiation Research Center (NSRRC, NSRRC, Taiwan light source). The S K-edge XAS spectra were measured at the beamline BL16A1 of NSRRC.

Electrochemical measurements

The HER performance of all the catalysts was evaluated by a three-electrode electrochemical system utilizing a CHI-760E electrochemical workstation in 0.5 M H_2SO_4 (Sinopharm Chemical ReagentCo., Ltd, 95.0 %-98.0 %) at room temperature, in which the standard Ag/AgCl (saturated KCl solution) electrode as the reference electrode[3, 4], a graphite rod as the counter electrode and the nanoporous catalysts including np-MoS_2, P/np-MoS_2, Pt_{SA}/np-MoS_2, and Pt_{SA}, P/np-MoS_2 with loading of 0.5 mg cm^{-2} coated on the carbon cloth (1×1 cm^2) as the working electrode. During the experiment, all the potentials were calibrated with a Reversible Hydrogen Electrode (RHE) according to the Nernst equation ($E_{RHE} = E_{Ag/AgCl} + 0.0591 \times PH + 0.197$ V) and rectified manually via 95% iR compensation after the data collection ($E_{iR\text{-}corrected} = E_{original} - 95\% \times iR_s$, in which i and R_s are the current density and solution resistance, respectively). Polarization curves were measured by LSV with a scan rate of 5 mV s^{-1}, and the overpotentials of HER were evaluated

at a current density of 10 mA cm^{-2}. Tafel curves were obtained based on the equation (η = b × log j + a, in which b and j are the Tafel slope and current density, respectively). In addition, LSV and Tafel curve extraction were also performed on Pt_{SA}, P/np-MoS_2 at the scan rate of 1 mV s^{-1} to explore the effect of steady-state responses on the Tafel slope.[5] EIS was conducted with an amplitude of 10 mV from 10^6 to 10^{-1} Hz frequency range at the overpotential of 30 mV vs. RHE. The ECSA of catalysts was assessed by the C_{dl} acquired from the relevant CV curves in the non-Faradaic potential region of 0.3 to 0.4 V with scan rates from 10 to 100 mV s^{-1}. ECSA was computed according to the equation ($ECSA = \frac{C_{dl}}{C_s}$, Cs is the specific capacitance), where the value of C_{dl} is half the slope of the line derived from linear fitting. It was found that the C_s value on a flat surface is normally in the range of 20 to 60 μF cm^{-2}. In this paper, the Cs value was uniformly assumed as 60 μF cm^{-2} based on reported values.[6] The mass activity, namely current density normalized to the mass of Pt, was calculated based on the equation ($j_{mass} = \frac{j}{m_{Pt}}$). The stability of the catalyst was tested by chronopotentiometry with an applied potential of 24 mV and 1000 CV cycles. The Faradaic efficiency (FE) was calculated according to the equation ($FE = \frac{n_e}{n_t}$), where n_e is the amount of experimentally determined H_2, n_t is the theoretically expected H_2 from the reaction. n_t was calculated by applying Faraday Law ($n_t = \frac{JAt}{2F}$), where J is current density, A is the electrode area, t is time in seconds, 2 is number of the electrons, and F is the Faraday constant (96485.4 C/mol).[7] FE is conducted under galvanostatic electrolysis at a current density of –10 mA cm^{-2}. H_2 generated from the reaction was collected by the water drainage method. The volume of H_2 produced was measured at different time intervals up to 60 min.

The PEMWE was constructed by assembling a self-made battery consisting of two polymethyl methacrylate panels. The obtained sheet catalyst supported on Ti cloth (2 × 2 cm^2) acted as the cathode. The commercial IrO_2 (20 wt%) sprayed on carbon cloth (2 × 2 cm^2) acted as the anode. The anode and

cathode were adhered together with the Nafion 117 membrane by heat pressing with a pressure of 2 MPa at 80 °C for 8 h as the membrane electrode in the PEMWE. All electrochemical tests were performed in 0.5 M H_2SO_4 electrolyte.

The ECSA of np-MoS_2, P/np-MoS_2, Pt_{SA}/np-MoS_2, and Pt_{SA}, P/np-MoS_2 were calculated as follow:

$$A_{ECSA}^{np-MoS_2} = \frac{47\ mF\ cm^{-2}}{2 \times 60\ \mu F\ cm^{-2}\ per\ cm_{ECSA}^2} = 391.67\ cm_{ECSA}^2$$

$$A_{ECSA}^{P/np-MoS_2} = \frac{71\ mF\ cm^{-2}}{2 \times 60\ \mu F\ cm^{-2}\ per\ cm_{ECSA}^2} = 591.67\ cm_{ECSA+}^2$$

$$A_{ECSA}^{Pt/np-MoS_2} = \frac{130\ mF\ cm^{-2}}{2 \times 60\ \mu F\ cm^{-2}\ per\ cm_{ECSA}^2} = 1083.33\ cm_{ECSA}^2$$

$$A_{ECSA}^{Pt,P/np-MoS_2} = \frac{141\ mF\ cm^{-2}}{2 \times 60\ \mu F\ cm^{-2}\ per\ cm_{ECSA}^2} = 1175.00\ cm_{ECSA}^2$$

The mass activity of Pt_{SA}/np-MoS_2, Pt_{SA}, P/np-MoS_2 and commercial Pt/C (20 wt%) were calculated as follow:

$$j_{mass}^{Pt_{SA}/np-MoS_2} = \frac{2.50\ mA\ cm^{-2}}{10.24\ ug\ cm^{-2}} = 0.24\ A\ mg^{-1}$$

$$j_{mass}^{Pt_{SA},P/np-MoS_2} = \frac{61.17\ mA\ cm^{-2}}{10.24\ ug\ cm^{-2}} = 5.97\ A\ mg^{-1}$$

$$j_{mass}^{Pt/C} = \frac{29.15\ mA\ cm^{-2}}{50.63\ ug\ cm^{-2}} = 0.58\ A\ mg^{-1}$$

DFT calculations

All computations were conducted employing DFT methods using the Vienna Ab initio Simulation Package (VASP 5.4.4)[8, 9]. The generalized gradient approximation of Perdew-Burke-Ernzerhof (GGA-PBE) was used to describe the exchange-correlation function. The basis set utilized the projector-augmented-wave pseudopotential (PAW) method, and the plane-wave energy cutoff was set at 500 eV[10, 11]. The MoS_2 of 2H or 1T were modeled by single-layer slabs with a (4×4) supercell, and the Monkhorst-Pack k-point sampling in the Brillouin zone was set to a (3 × 3 × 1) for calculations. Convergence was

assumed when forces on each atom were less than 0.02 eV/Å and the self-consistent field (SCF) tolerance was 10^{-6} eV in the geometry optimization. To avoid the interactions between periodic structures, the vacuum space was set to 20 Å. The DFT-D3 method with Grimme's scheme was employed to correct the van der Waals interactions[12]. The Gibbs free energy of hydrogen adsorption ($^{\Delta G_{ad}(*H)}$) was calculated by

$$G_{ad}(*H) = E(Slab+H) - E(Slab) - \frac{1}{2} * E(H_2) + \Delta ZPE - T\Delta S + \Delta H$$

where $\Delta ZPE - T\Delta S + \Delta H$ for HER is about 0.24 eV[13].

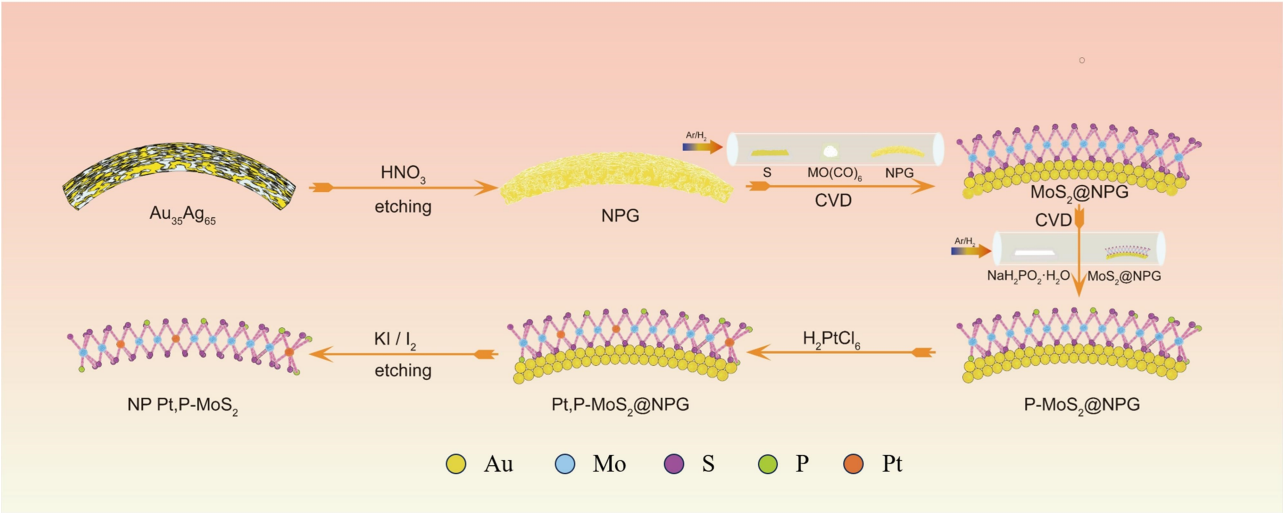

Figure S1. Schematic illustration of synthesis process for Pt_{SA}, P/np-MoS_2.

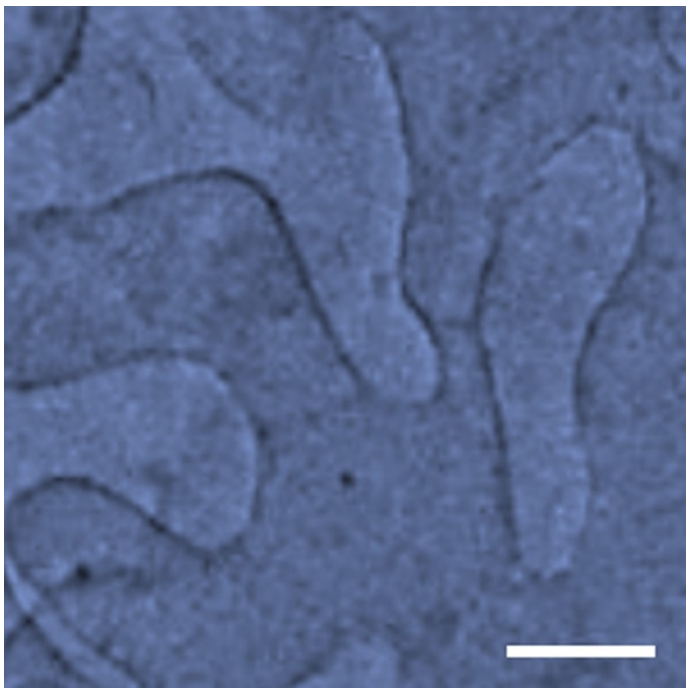

Figure S2. A typical TEM image of the as-prepared Pt_{SA}, P/np-MoS_2, showing the nanotube-shaped Ligaments. Scale bar: 200 nm.

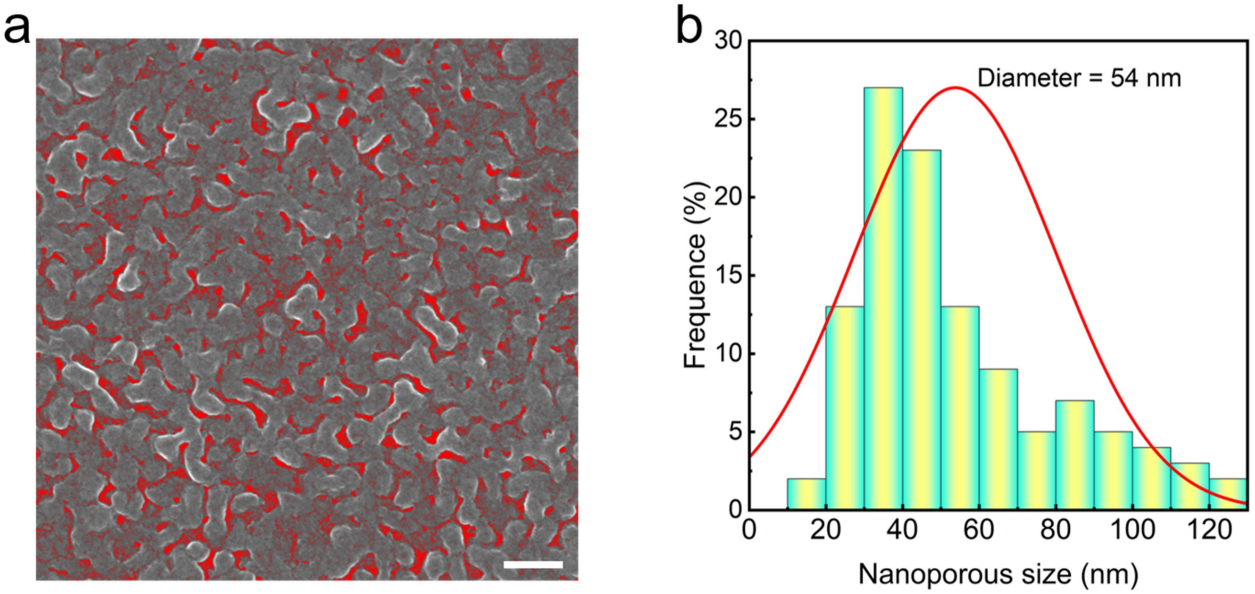

Figure S3. (a) A typical SEM image of the as-prepared Pt_{SA}, P/np-MoS_2. (b) The average pore diameter is measured to be 54 nm from (a). Scale bar: 100 nm.

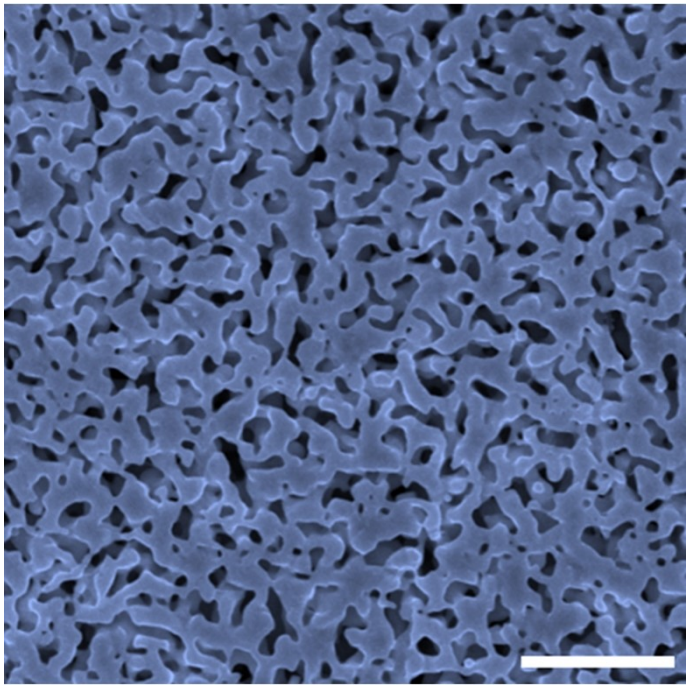

Figure S4. SEM characterizations of Pt_{SA}, P/np-MoS_2@NPG. Scale bar: 1 um.

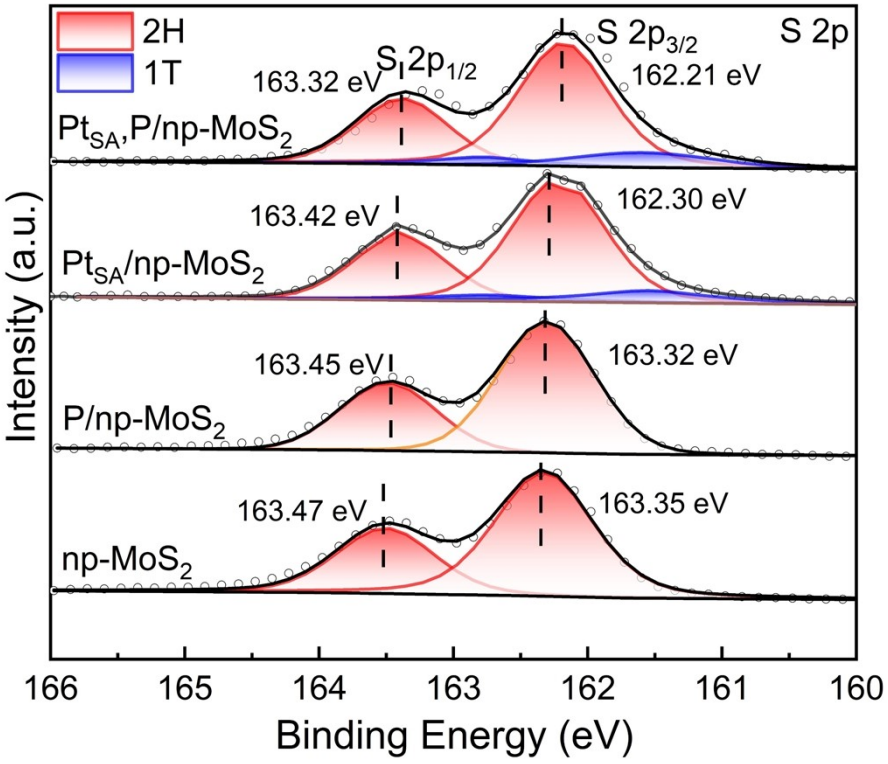

Figure S5. High-resolution XPS spectra of S 2p belong to np-MoS_2, P/np-MoS_2, Pt_{SA}/np-MoS_2, and Pt_{SA}, P/np-MoS_2.

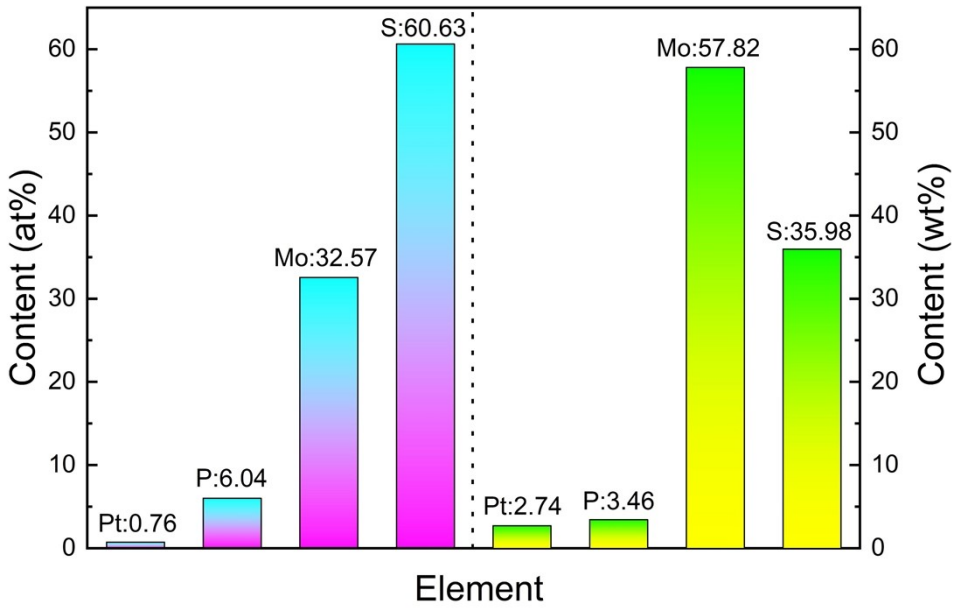

Figure S6. ICP-OES analysis of Pt_{SA}, P/np-MoS_2. The Pt content is very low.

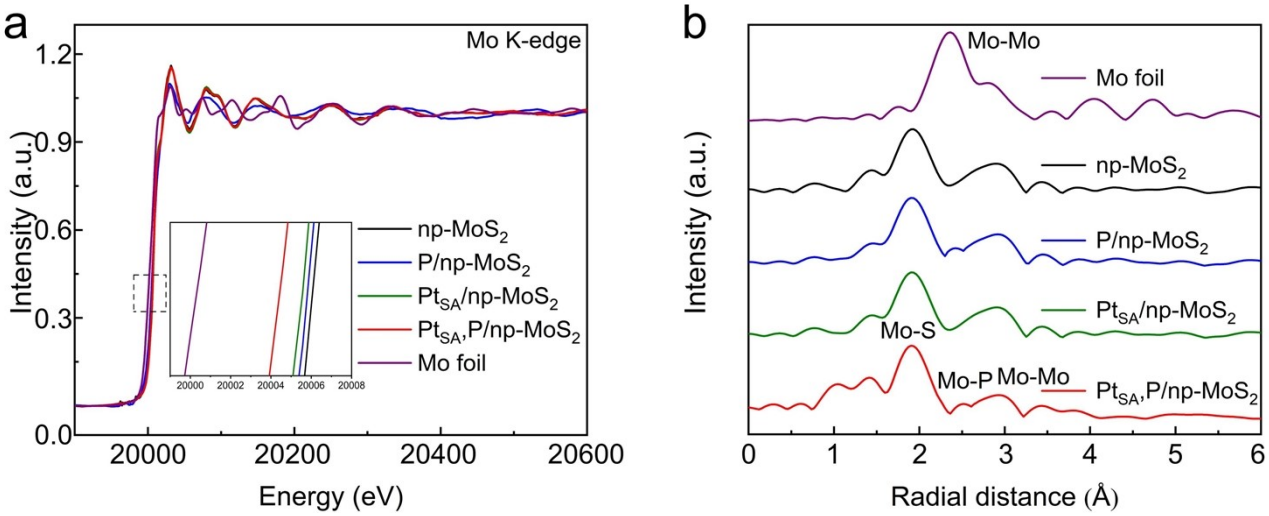

Figure S7. (a) Mo K-edge XANES spectra of np-MoS_2, P/np-MoS_2, Pt_{SA}/np-MoS_2, Pt_{SA}, P/np-MoS_2, and Mo foil. (b) Corresponding FT-EXAFS spectra from (a).

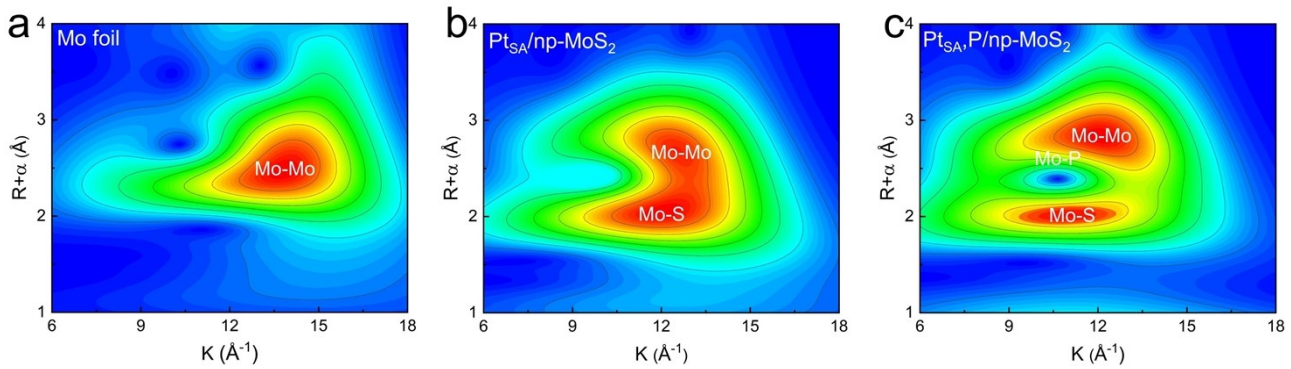

Figure S8. Wavelet transforms of (a) Mo foil, (b) Pt_{SA}/np-MoS_2, and (c) Pt_{SA}, P/np-MoS_2.

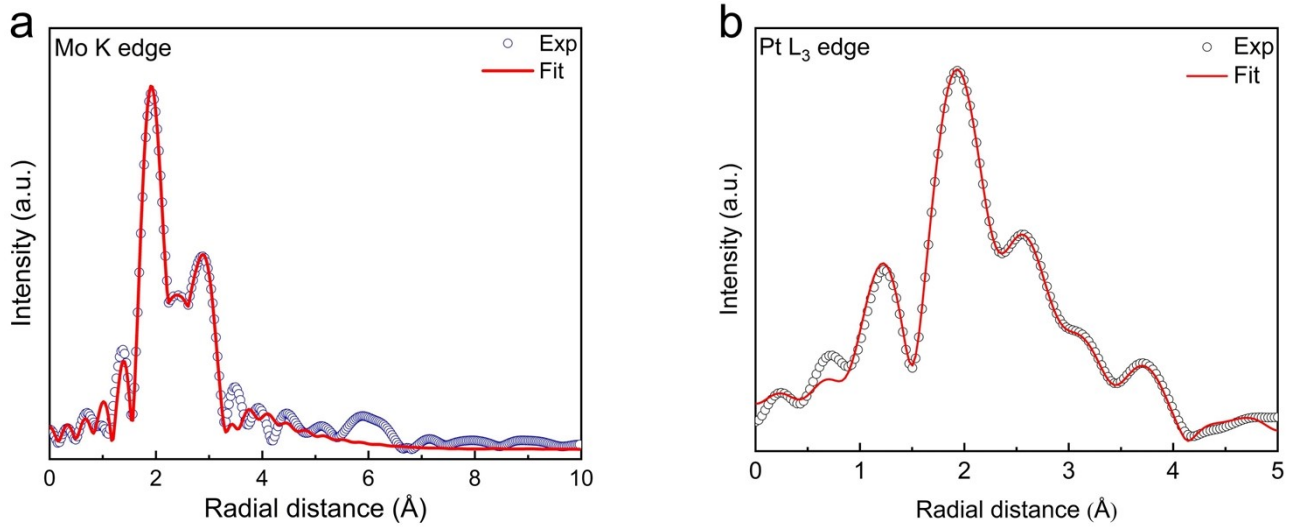

Figure S9. The fitting FT-EXAFS of (a) Mo K-edge and (b) Pt L_3-edge in Pt_{SA}, P/np-MoS_2 with the different fitting paths.

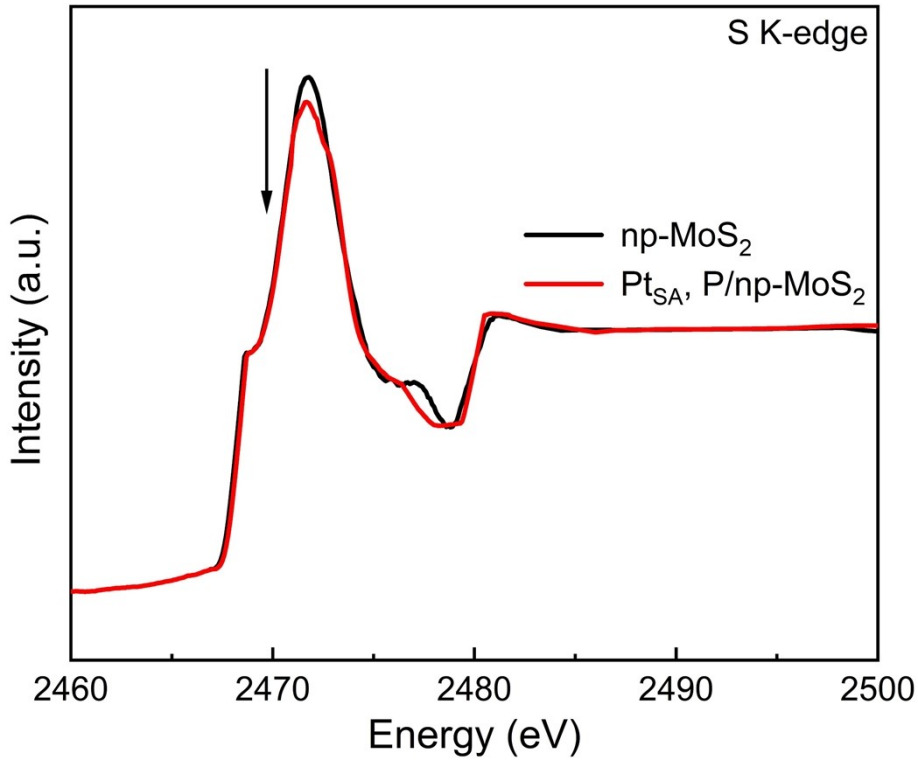

Figure S10. S K-edge XANES spectra of np-MoS_2 and Pt_{SA}, P/np-MoS_2.

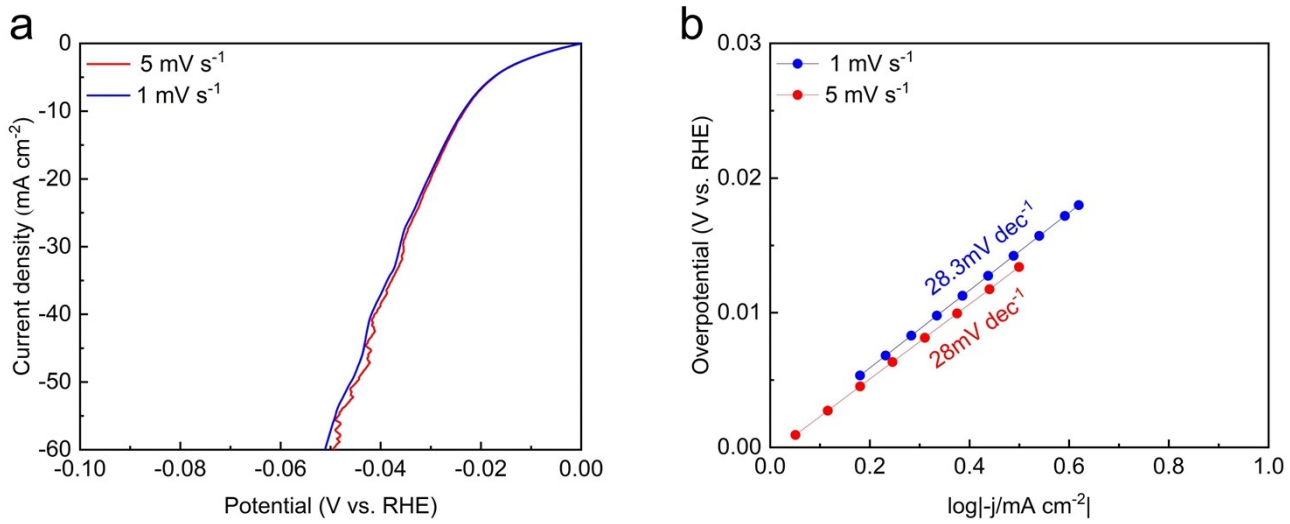

Figure S11. (a) HER polarization curves of Pt_{SA}, P/np-MoS_2 at different scan rates. (b) Corresponding Tafel plots derived from (a).

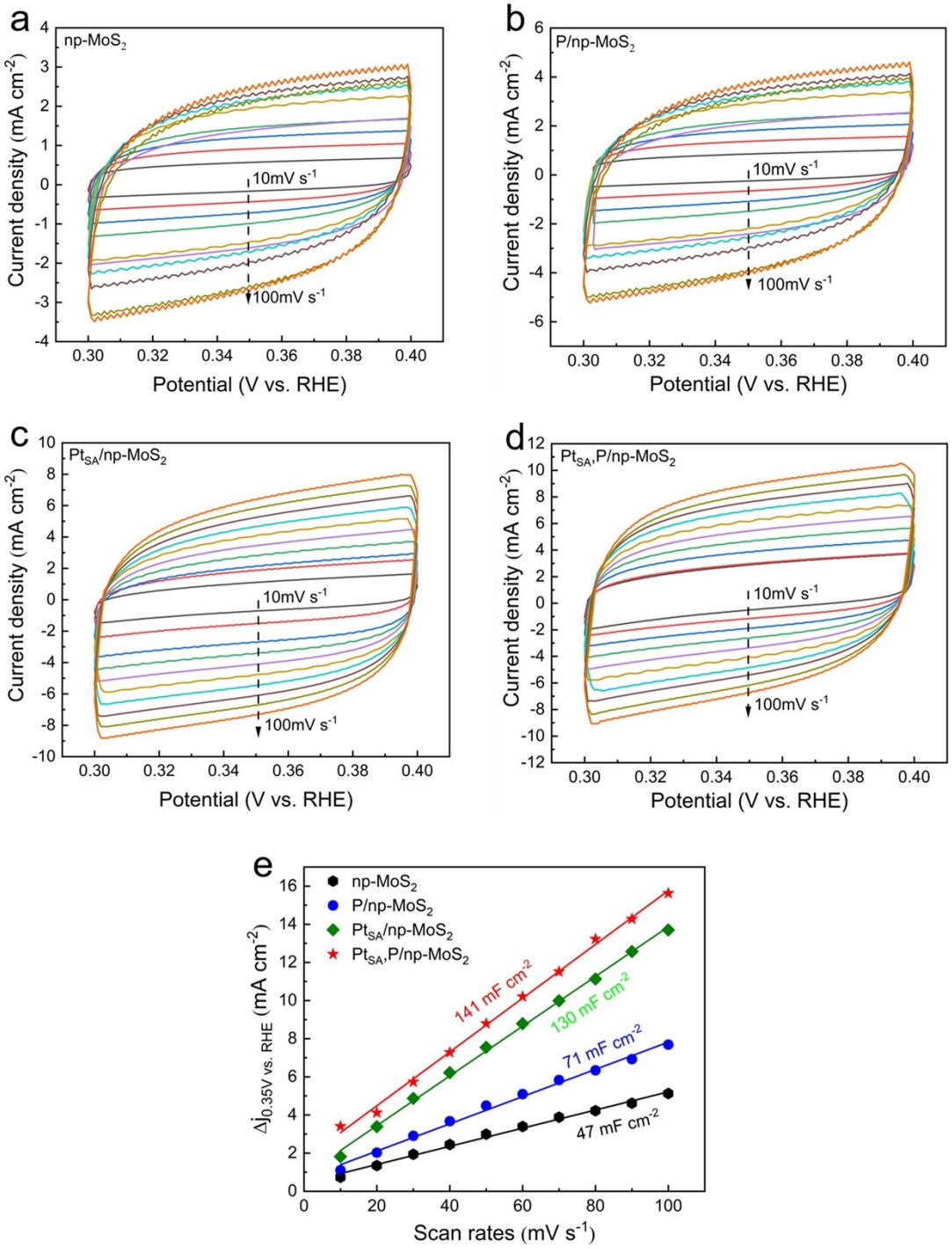

Figure S12. CV curves at various scan rates (10, 20, 30, 40, 50, 60, 70, 80, 90, and 100 mV s^{-1}) of (a) np-MoS_2, (b) P/np-MoS_2, (c) Pt_{SA}/np-MoS_2, (d) Pt_{SA}, P/np-MoS_2 in 0.5M H_2SO_4 solution at the potential range of 0.30 to 0.40 V (vs. RHE). (e) The scaling relationship between Δj (the difference between anodic and cathodic current densities at 0.35 V) and scan rates for np-MoS_2, P/np-MoS_2, Pt_{SA}/np-MoS_2, and Pt_{SA}, P/np-MoS_2.

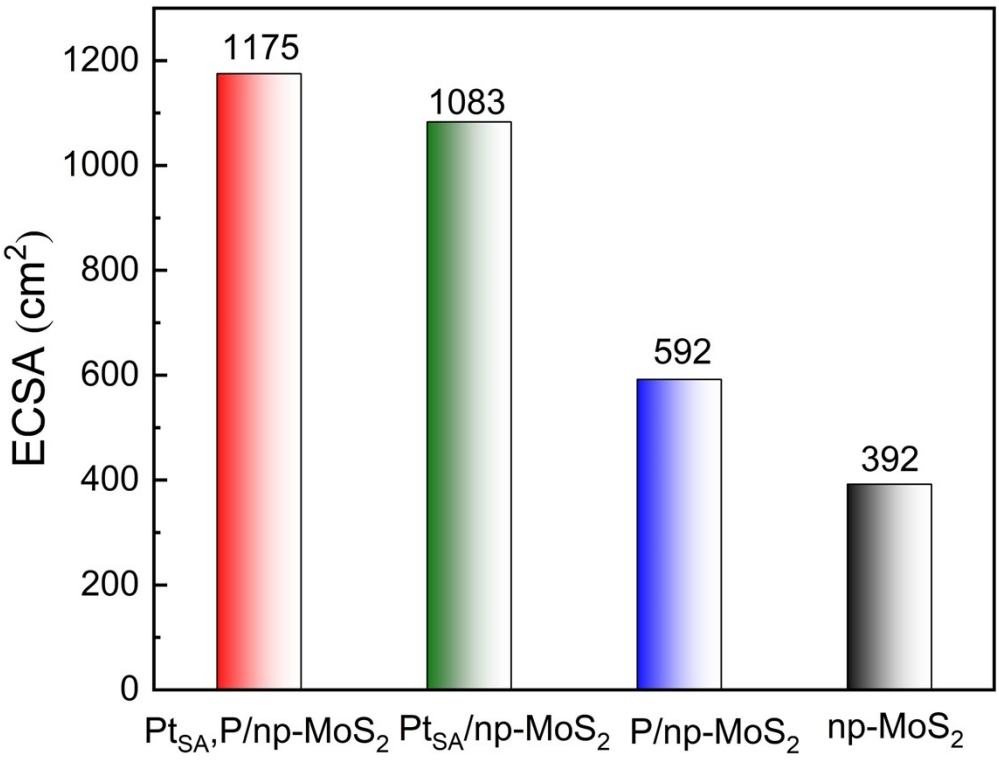

Figure S13. The real ECSA of np-MoS_2, P/np-MoS_2, Pt_{SA}/np-MoS_2, and Pt_{SA}, P/np-MoS_2.. The ECSA value was calculated based on the equation of $ECSA=C_{dl}/C_s$, where C_s is the specific capacitance. In this work, the C_s is assumed as 60 μF cm^{-2}.

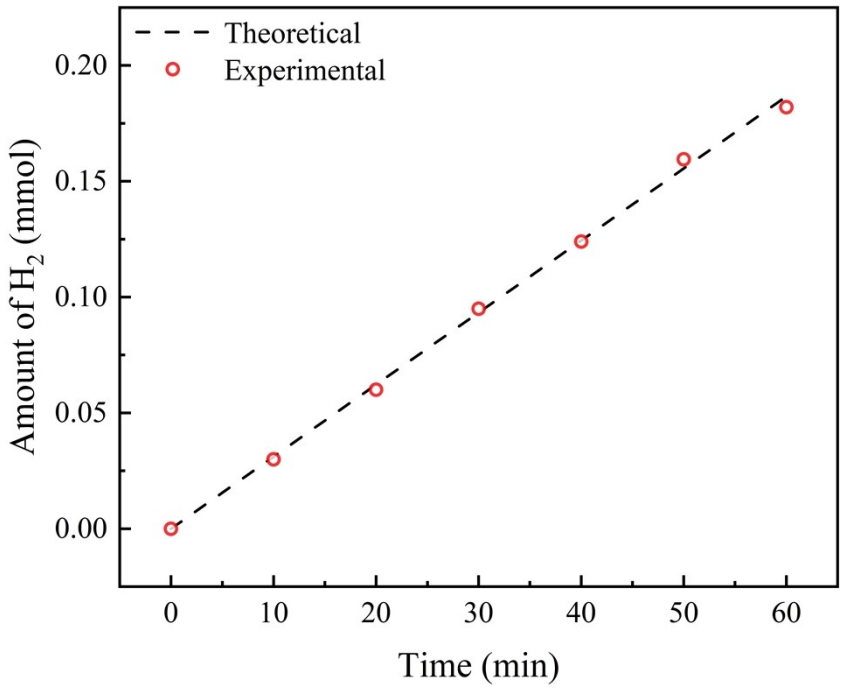

Figure S14. Faradaic efficiency of hydrogen evolution of Pt_{SA}, P/np-MoS_2.

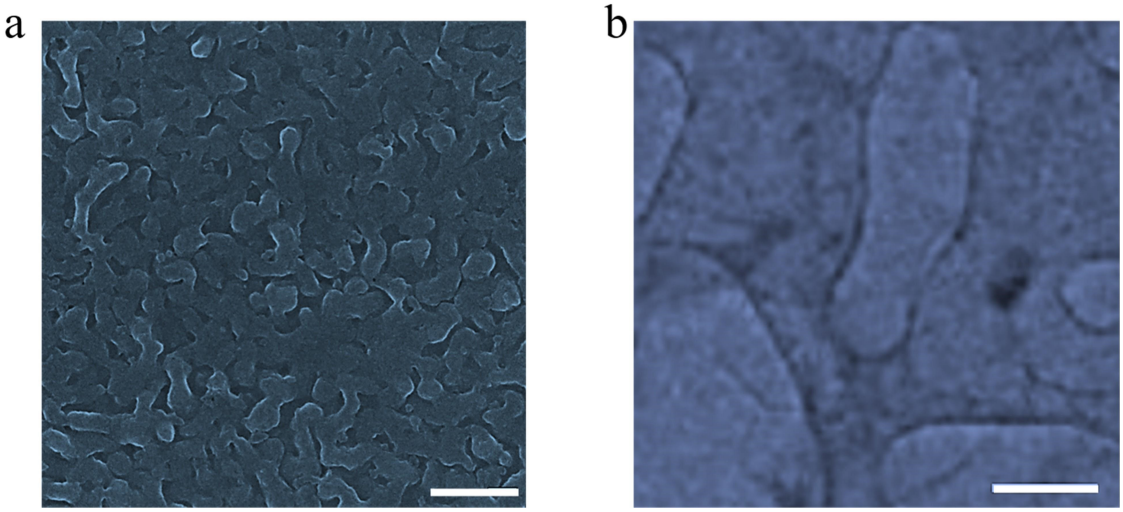

Figure S15. The (a) SEM image and (b) TEM image of Pt_{SA}, P/np-MoS_2 after HER test for 100 h. Scale bar: (a) 300 nm (b) 200 nm.

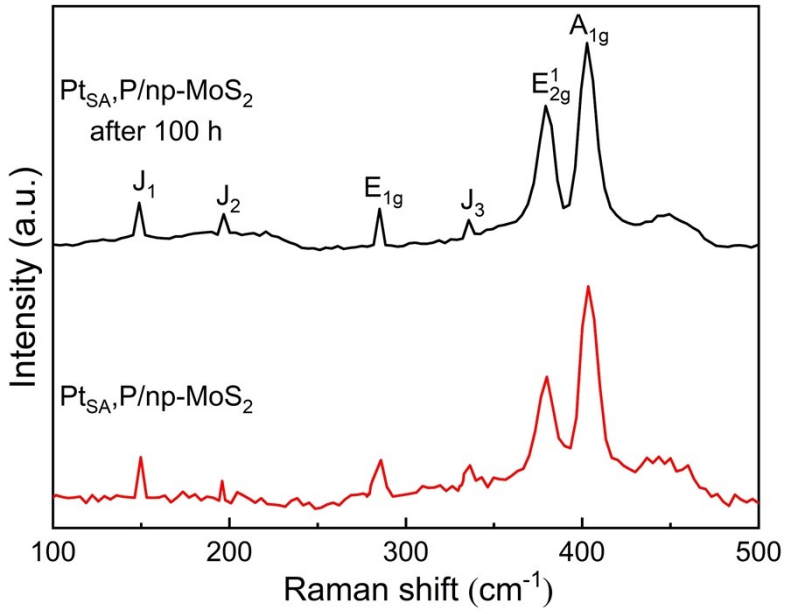

Figure S16. The Raman spectra of initial Pt_{SA}, P/np-MoS_2 and Pt_{SA}, P/np-MoS_2 after cycling 100 h.

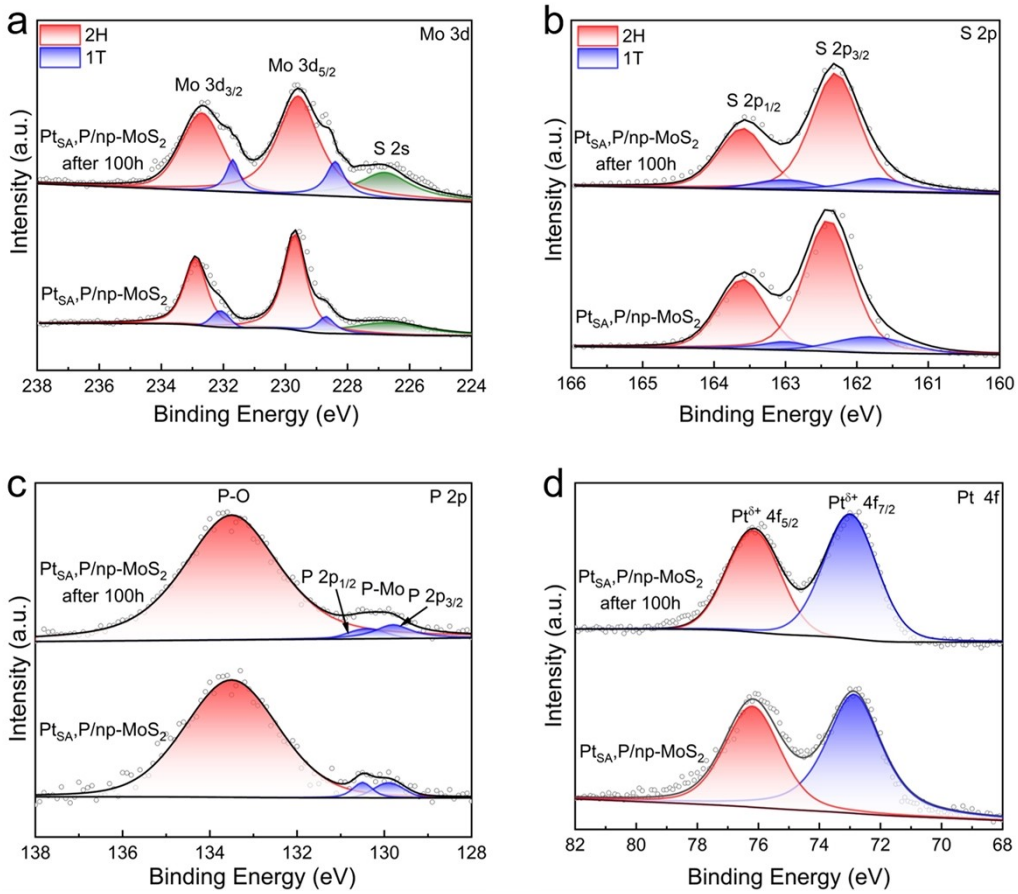

Figure S17. High-resolution XPS spectra of initial and final (after cycling 100 h) (a) Mo 3d, (b) S 2p, (c) P 2p, and (d) Pt 4f.

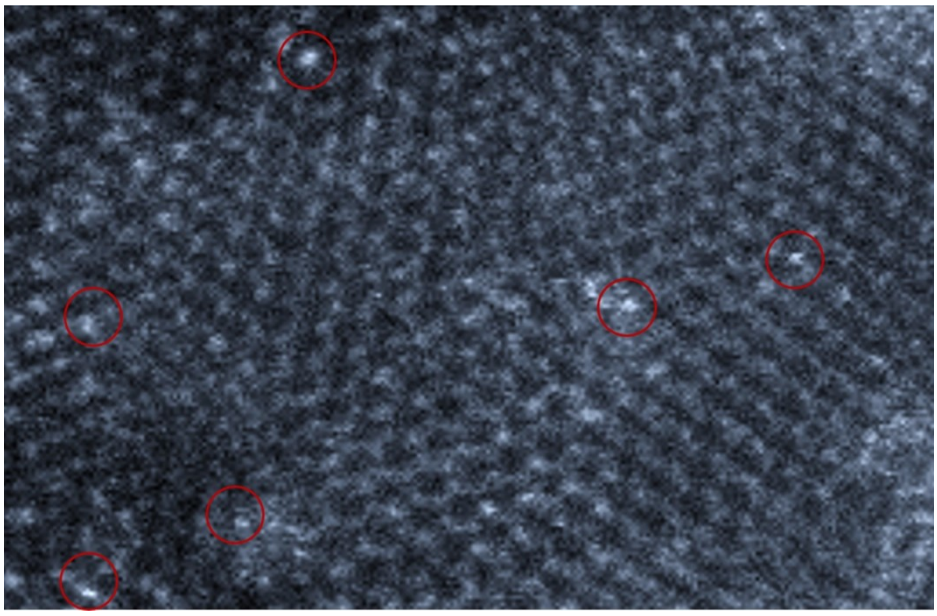

Figure S18. Magnified HAADF-STEM image of Pt_{SA}, P/np-MoS_2 after cycling 100 h, showing the existence of isolated Pt atoms (red circles). Scale bar: 2 nm

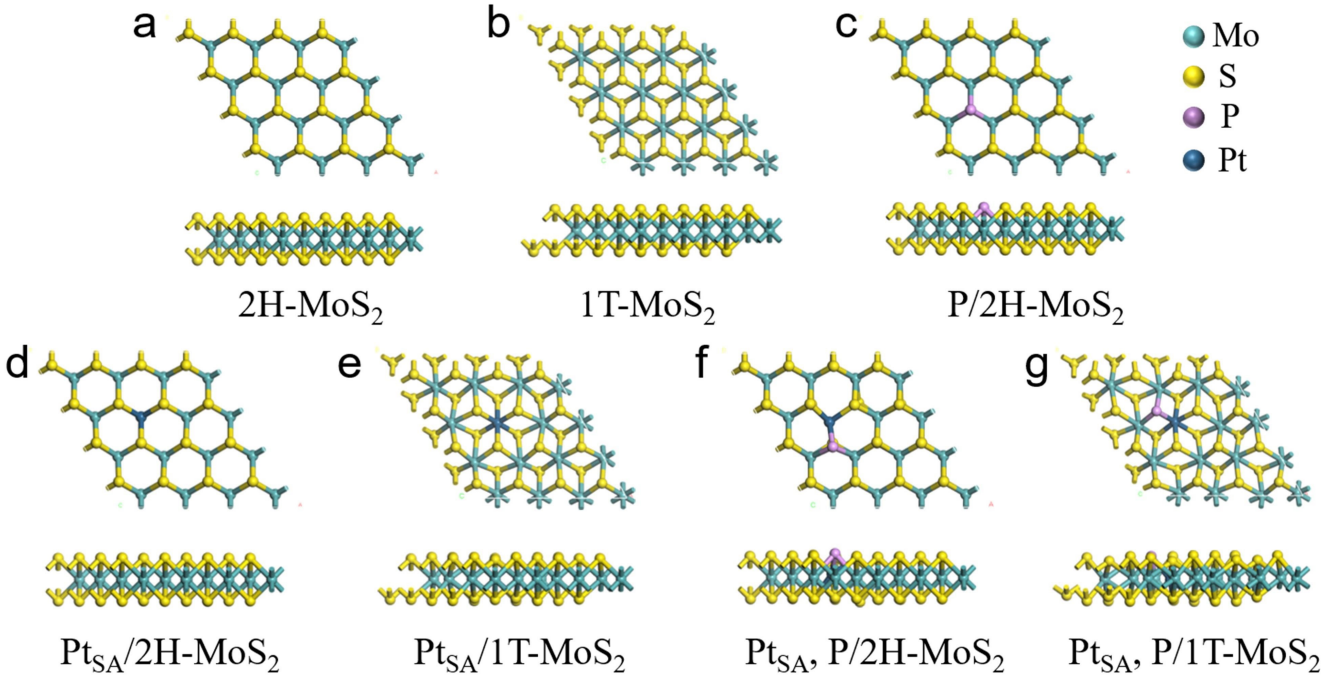

Figure S19. Optimized atomic configurations of top-view and side-view structures of (a) 2H-MoS_2, (b) 1T-MoS_2, (c) P/2H-MoS_2, (d) Pt_{SA}/2H-MoS_2, (e) Pt_{SA}/1T-MoS_2, (f) Pt_{SA}, P/2H-MoS_2, (g) Pt_{SA}, P/1T-MoS_2.

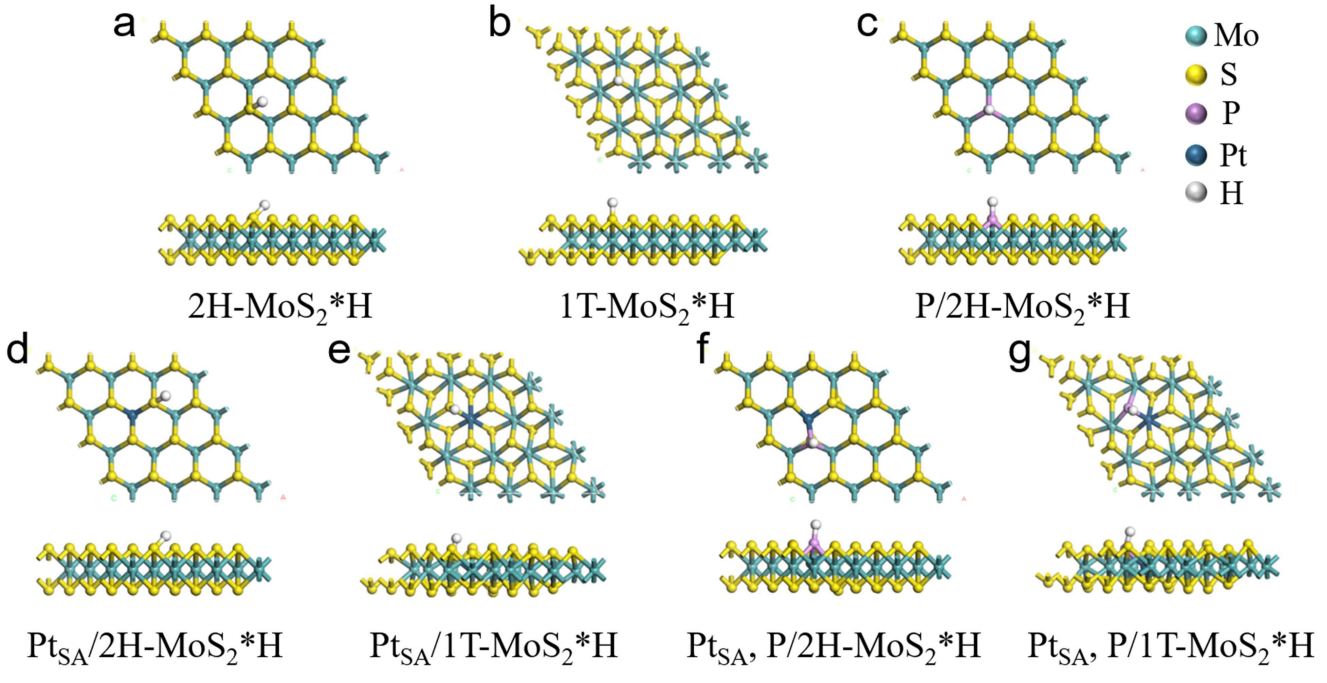

Figure S20. H* adsorption on (a) 2H-MoS_2, (b) 1T-MoS_2, (c) P/2H-MoS_2, (d) Pt_{SA}/2H-MoS_2, (e) Pt_{SA}/1T-MoS_2, (f) Pt_{SA}, P/2H-MoS_2, (g) Pt_{SA}, P/1T-MoS_2.

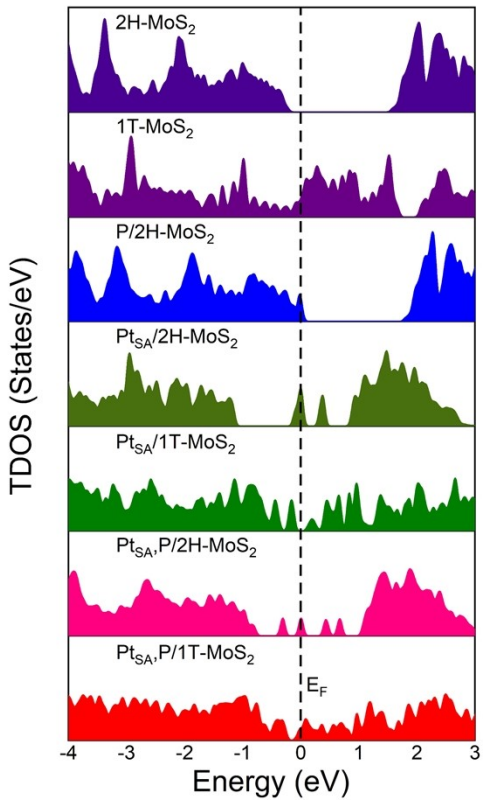

Figure S21. TDOS distribution of 2H-MoS_2, 1T-MoS_2, P/2H-MoS_2, Pt_{SA}/2H-MoS_2, Pt_{SA}/1T-MoS_2, Pt_{SA}, P/2H-MoS_2, Pt_{SA}, P/1T-MoS_2.

Table S1. The atomic ratio and weight ratio data of all elements in np-MoS_2, P/np-MoS_2, Pt_{SA}/np-MoS_2, and Pt_{SA}, P/np-MoS_2 from XPS result.

Catalysts	np-MoS_2		P/np-MoS_2			Pt_{SA}/np-MoS_2			Pt_{SA}, P/np-MoS_2			
Elements	Mo	S	P	Mo	S	Pt	Mo	S	Pt	P	Mo	S
Atomic %	34.56	65.44	7.12	33.24	59.64	0.74	34.15	65.11	0.74	6.94	32.07	60.25
Weight %	61.25	48.75	4.14	59.93	35.93	2.62	59.48	37.90	2.69	4.00	57.32	35.99

Table S2. Structural parameters extracted from the EXAFS fitting of Pt_{SA}, P/np-MoS_2.

Catalysts	Scattering path	CN	R (Å)	$\sigma^2(10^{-3}$ Å$^2)$	❒E_0 (eV)	R-factor
Pt_{SA}, P/np-MoS_2	Mo-S	5.49	2.41	3.18	3.82	0.01
	Mo-P	5.23	2.52	3.06	3.15	0.01
	Mo-Mo	6.21	3.17	4.24	1.56	0.01

Pt_{SA}, P/np-MoS_2	Pt-P/S	3.6	2.09	5.13	4.064	0.0053

Note: CN represents the coordination number; R represents the interatomic distance; σ^2 represents the Debye-Waller factor; ΔE_0 represents the edge-energy shift.

Table S3. Comparison of overpotential at 10 mA cm^{-2} and Tafel slope of Pt_{SA}, P/np-MoS_2 with recently reported MoS_2-based catalysts in 0.5 M H_2SO_4.

Catalysts	Electrolyte	η@10mA cm^{-2} (mV)	Tafel slope (mV dec^{-1})	Reference
Pt_{SA}, P/np-MoS_2	0.5 M H_2SO_4	30	29	This work
MCM@MoS_2–Ni	0.5 M H_2SO_4	53	81	(6)[14]
CoS_2@WS_2/CC	0.5 M H_2SO_4	97.2	66.0	(7)[15]
Pd, Re-MoS_2	0.5 M H_2SO_4	46	72	(8)[16]
Cu-Pd-MoS_2	0.5 M H_2SO_4	93	74	(9)[17]
P, Se-MoS_2/CNTs	0.5 M H_2SO_4	110	49	(10)[18]
1% Pd-MoS_2/CC	0.5 M H_2SO_4	78	62	(11)[19]
Pt@MoS_2	0.5 M H_2SO_4	88.43	55.69	(12)[20]
MoS_2 ML	0.5 M H_2SO_4	90	94	(13)[21]

MoS_2/Graphene	0.5 M H_2SO_4	110	67.4	(14)[22]
Ni2P/MoS_2/N:RGO	0.5 M H_2SO_4	39.5	39.52	(15)[23]
P-MoS_2@HCMF	0.5 M H_2SO_4	86	42.35	(16)[24]
MoS_2@Pt-3	0.5 M H_2SO_4	70	36	(17)[25]
CoFe@NDC@MoS_2	0.5 M H_2SO_4	64	45	(18)[26]

References

1. Y. Tan, P. Liu, L. Chen, W. Cong, Y. Ito, J. Han, X. Guo, Z. Tang, T. Fujita, A. Hirata and M. W. Chen, *Adv. Mater.*, 2014, **26**, 8023-8028.
2. D. Chen, Z. Wei, M. Wang, S. Zhao, P. Liu, A. Pan and Y. Tan, *Nano Lett.*, 2022, **22**, 7020-7027.
3. Y.-C. Chen, A.-Y. Lu, P. Lu, X. Yang, C.-M. Jiang, M. Mariano, B. Kaehr, O. Lin, A. Taylor, I. D. Sharp, L.-J. Li, S. S. Chou and V. Tung, *Adv. Mater.*, 2017, **29**, 1703863.
4. D. Voiry, R. Fullon, J. Yang, C. de Carvalho Castro e Silva, R. Kappera, I. Bozkurt, D. Kaplan, M. J. Lagos, P. E. Batson, G. Gupta, Aditya D. Mohite, L. Dong, D. Er, V. B. Shenoy, T. Asefa and M. Chhowalla, *Nat Mater*, 2016, **15**, 1003-1009.
5. S. Anantharaj, S. Noda, M. Driess and P. W. Menezes, *Acs Energy Lett*, 2021, **6**, 1607-1611.
6. D. Chen, R. Lu, R. Yu, Y. Dai, H. Zhao, D. Wu, P. Wang, J. Zhu, Z. Pu, L. Chen, J. Yu and S. Mu, *Angew. Chem. Int. Ed.*, 2022, **61**, e202208642.
7. J. Li, Y. Li, J. Wang, C. Zhang, H. Ma, C. Zhu, D. Fan, Z. Guo, M. Xu, Y. Wang and H. Ma, *Adv. Funct. Mater.*, 2022, **32**, 2109439.

8. G. Kresse and J. Furthmüller, *Phys. Rev. B*, 1996, **54**, 11169.

9. J. P. Perdew, K. Burke and M. Ernzerhof, *Phys. Rev. Lett.*, 1996, **77**, 3865.

10. P. E. Blöchl, *Phys. Rev. B*, 1994, **50**, 17953-17979.

11. G. Kresse and D. Joubert, *Phys. Rev. B*, 1999, **59**, 1758.

12. S. Grimme, J. Antony, S. Ehrlich and H. Krieg, *J. Chem. Phys.*, 2010, **132**, 154104.

13. E. Santos, P. Quaino and W. Schmickler, *Phys. Chem. Chem. Phys.*, 2012, **14**, 11224-11233.

14. H. B. Zhang, L. Yu, T. Chen, W. Zhou and X. W. Lou, *Adv. Funct. Mater.*, 2018, **28**, 1807086.

15. X. F. Zhou, X. L. Yang, H. N. Li, M. N. Hedhili, K. W. Huang, L. J. Li and W. J. Zhang, *J. Mater. Chem. A*, 2017, **5**, 15552-15558.

16. Z. Y. Luo, J. J. Li, Y. L. Li, D. J. Wu, L. Zhang, X. Z. Ren, C. X. He, Q. L. Zhang, M. Gu and X. L. Sun, *Adv. Energy Mater.*, 2022, **12**, 2103823.

17. D. C. Han, Z. Y. Luo, Y. Li, N. X. Gao, J. J. Ge, C. P. Liu and W. Xing, *Appl. Surf. Sci.*, 2020, **529**, 147117.

18. T. Zhu, J. B. Ding, Q. Shao, Y. Qian and X. Q. Huang, *Chemcatchem*, 2019, **11**, 689-692.

19. Z. Y. Luo, Y. X. Ouyang, H. Zhang, M. L. Xiao, J. J. Ge, Z. Jiang, J. L. Wang, D. M. Tang, X. Z. Cao, C. P. Liu and W. Xing, *Nat. Commun.*, 2018, **9**, 2120.

20. Y. Li, Q. F. Gu, B. Johannessen, Z. Zheng, C. Li, Y. T. Luo, Z. Y. Zhang, Q. Zhang, H. I. Fan, W. B. Luo, B. L. Liu, S. X. Dou and H. K. Liu, *Nano Energy*, 2021, **84**, 105898.

21. J. Qu, Y. Li, F. Li, T. M. Li, X. Y. Wang, Y. Yin, L. B. Ma, O. G. Schmidt and F. Zhu, *Acs Nano*, 2022, **16**, 2921-2927.

22. L. B. Ma, Y. Hu, G. Y. Zhu, R. P. Chen, T. Chen, H. L. Lu, Y. R. Wang, J. Liang, H. X. Liu, C. Z. Yan, Z. X. Tie, Z. Jin and J. Liu, *Chem. Mater.*, 2016, **28**, 5733-5742.

23. M. Kim, M. A. R. Anjum, M. Lee, B. J. Lee and J. S. Lee, *Adv. Funct. Mater.*, 2019, **29**, 1809151.

24. J. Xiong, J. Li, J. W. Shi, X. L. Zhang, W. W. Cai, Z. H. Yang and H. S. Cheng, *Appl Catal B-Environ*, 2019, **243**, 614-620.

25. X. Y. Xu, X. F. Dong, Z. J. Bao, R. Wang, J. G. Hu and H. B. Zeng, *J. Mater. Chem. A*, 2017, **5**, 22654-22661.

26. S. Ali Shah, L. Xu, R. Sayyar, T. Bian, Z. Liu, A. Yuan, X. Shen, I. Khan, A. Ali Tahir and H. Ullah, *Chem. Eng. J.*, 2022, **428**, 132126.